Thermodynamic stability of nanosized multicomponent bubbles/droplets: The square gradient theory and the capillary approach

Øivind Wilhelmsen, Dick Bedeaux, Signe Kjelstrup, and David Reguera

Citation: The Journal of Chemical Physics **140**, 024704 (2014); doi: 10.1063/1.4860495
View online: http://dx.doi.org/10.1063/1.4860495
View Table of Contents: http://scitation.aip.org/content/aip/journal/jcp/140/2?ver=pdfcov
Published by the AIP Publishing

Thermodynamic stability of nanosized multicomponent bubbles/droplets: The square gradient theory and the capillary approach

Øivind Wilhelmsen,[1,a)] Dick Bedeaux,[1] Signe Kjelstrup,[1] and David Reguera[2]
[1]*Department of Chemistry, Norwegian University of Science and Technology, Trondheim, Norway*
[2]*Departament de Física Fonamental, Universitat de Barcelona, Martí i Franquès 1, Barcelona, Spain*

(Received 17 October 2013; accepted 16 December 2013; published online 10 January 2014)

Formation of nanosized droplets/bubbles from a metastable bulk phase is connected to many unresolved scientific questions. We analyze the properties and stability of multicomponent droplets and bubbles in the canonical ensemble, and compare with single-component systems. The bubbles/droplets are described on the mesoscopic level by square gradient theory. Furthermore, we compare the results to a capillary model which gives a macroscopic description. Remarkably, the solutions of the square gradient model, representing bubbles and droplets, are accurately reproduced by the capillary model except in the vicinity of the spinodals. The solutions of the square gradient model form closed loops, which shows the inherent symmetry and connected nature of bubbles and droplets. A thermodynamic stability analysis is carried out, where the second variation of the square gradient description is compared to the eigenvalues of the Hessian matrix in the capillary description. The analysis shows that it is impossible to stabilize arbitrarily small bubbles or droplets in closed systems and gives insight into metastable regions close to the minimum bubble/droplet radii. Despite the large difference in complexity, the square gradient and the capillary model predict the same finite threshold sizes and very similar stability limits for bubbles and droplets, both for single-component and two-component systems. © *2014 AIP Publishing LLC*. [http://dx.doi.org/10.1063/1.4860495]

I. INTRODUCTION

Small systems receive now increasing attention, not only in academia, but also in industry. Fabrication of novel nano materials, for instance, requires exquisite control and insight into phase transitions such as condensation, evaporation, and crystallization at the nanoscale. In industry, distillation columns, heat exchangers, and chemical reactors rely on sufficient transfer of heat and mass during phase transitions.[1,2] In nature, precipitation of rain is one of many phase transitions which initiates at the nanoscale.

The first and important step in a typical phase transition is the formation of a nucleus from a metastable bulk phase.[3] Recent experimental developments have made it possible to observe formation of tiny droplets and crystals consisting of only a few molecules.[4,5] Further growth can be limited by heat and mass transfer through the surface, which will be strongly affected by the curvature of mesoscopic nuclei.[6]

Classical Nucleation Theory (CNT) is still today the most popular theory to predict nucleation rates.[3,7,8] It succeeds in capturing the qualitative behavior, but fails to predict the correct temperature dependency of nucleation rates, and the predicted rates are often orders of magnitude different from measurements in unary and in multicomponent systems.[9–12] Molecular dynamics and Monte Carlo simulations are important sources of information on nucleation,[13–19] that for complicated mixtures and realistic conditions comes at the expense of large computational costs.[20]

In this work, we will give attention to square gradient theory, first formulated for single-component systems by van der Waals,[21] extended to mixtures by Cahn and Hillard[22] and to the non-equilibrium domain by Bedeaux and co-workers for single-component systems[23] and Glavatskiy and Bedeaux for mixtures.[24] Square gradient theory is the first approximation to density functional theory, and has successfully been used to predict both nucleation rates and non-equilibrium transport properties.[25–28] In many cases, it corrects some of the limitations and predicts nucleation rates more accurately than CNT. The computational time for mixtures is of the order of seconds, which makes the method attractive compared to molecular simulation techniques.

One of the main difficulties in the study of nucleation is the fact that the most important entity, the critical cluster, is unstable. Already in 1985, Yang[29] predicted that bubbles and droplets in single-component systems were thermodynamically unstable when connected to pressure and temperature reservoirs, or in open systems connected to thermal reservoirs (grand canonical ensemble). However, bubbles and droplets can be stable in closed systems connected to a thermal reservoir, i.e., the canonical ensemble (constant total mass of components, total volume, and temperature). Here, they represent minima of the system's Helmholtz energy. The thermodynamically stable clusters in this ensemble can be shown to correspond to condensing or evaporating nuclei in open systems.[30–32] Systems with bubbles/droplets in the canonical ensemble thus provide a way to investigate the properties of nanosized bubbles/droplets of interest for nucleation.

Square gradient theory, and density functional theory in general find constrained stationary states in the system's

a)Electronic mail: oivind.wilhelmsen@ntnu.no

Helmholtz energy (zero first functional derivatives), and pay no attention to whether this corresponds to maxima, minima, or saddle points. There are many ways to investigate thermodynamic stability. Some authors evaluate the stability of bubbles/droplets by comparing the difference in the Helmholtz energy of the composite system with that of a system at homogeneous density, referred to as the reversible work of formation of the bubble/droplet.[33,34] This identifies the phase with the lowest Helmholtz energy but does not give rigorous answers about the nature and stability of the different stationary solutions.

In the capillary model, thermodynamic stability can be evaluated through the eigenvalues of the Hessian matrix. Since the Helmholtz energy is a function of a finite number of variables, the method gives a finite number of eigenvalues, where all are positive in a stable system. It is more difficult to examine stability of the square gradient model, or density functional formulations in general. A thermodynamically stable configuration is here characterized by a second variation of the Helmholtz energy functional which has to be positive for all feasible density fluctuations. The complexity of the second order functional derivatives makes it difficult to prove thermodynamic stability in functional representations.[29]

For single-component systems with simplified expressions for the Helmholtz energy, the problem has been addressed by several authors by taking advantage of the similarity between the second variation of the square gradient model and the eigenvalue problem of the Schrödinger equation.[35–38] With orthogonal eigenfunctions, the second variation is quadratic in the eigenfunctions and stability is decided by the sign of the eigenvalues. Unlike in the capillary model, there is an infinite number of eigenvalues. For a realistic choice of the Helmholtz energy, the problem cannot be solved analytically, which makes the methodology unfeasible.

In this work, we use a perturbation approach to address the thermodynamic stability of bubbles/droplets in the square gradient model coupled with an accurate cubic equation of state.[24,39–41] We discuss the behavior of single-component systems and mixtures. The results are compared to a similar analysis with the capillary model. Despite the large difference in complexity, we show that these two approaches predict very similar stability limits also for mixtures. This has to the best of our knowledge, not been shown before.

The paper is structured as follows. The theoretical framework is presented in Sec. II. A short introduction is given to the square gradient theory (mesoscopic approach), the capillary approach (macroscopic approach), and the framework to analyze the thermodynamic stability. We present the cases considered and our findings in Sec. III. Finally, concluding remarks are provided in Sec. IV.

II. THEORY

Consider a spherical container with radius R_{tot}, volume, V_{tot}, temperature, T, and a fixed number of moles of components i, $N_{\text{tot,i}}$. We assume that a perfectly spherical bubble or droplet with radius R_n is placed at the center of the container as depicted in Fig. 1.

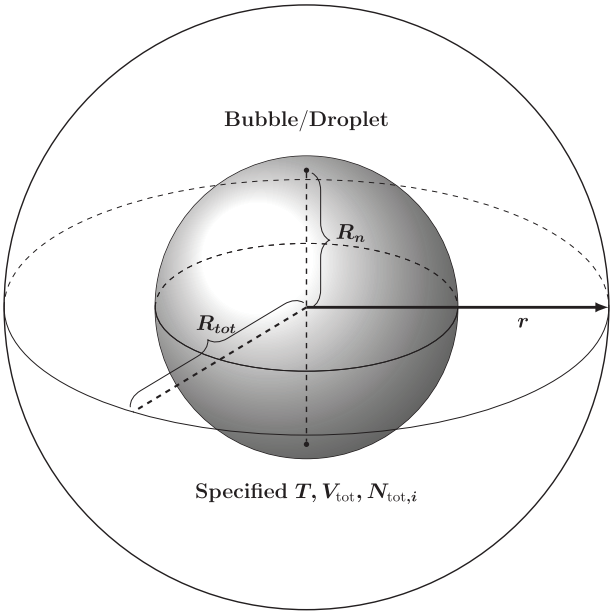

FIG. 1. Illustration of the system investigated.

Both the square gradient model and the capillary approach rely on an equation of state which is capable of capturing the thermodynamic behavior of both the liquid and the vapor at different compositions. In this work, we use the Peng-Robinson cubic equation of state, which has proven to give accurate predictions of the density and vapor-liquid equilibrium properties in both gas and liquid regions for non-polar mixtures.[39–41] Cubic equations of state can be represented as

$$P_{\text{eos}} = \frac{R_g T}{v-b} - \frac{a\alpha(T)}{(v-bm_1)(v-bm_2)}. \tag{1}$$

Here, P_{eos} is the pressure predicted by the equation of state, R_g the universal gas constant, v the molar volume, and a, α, and b are parameters of the equation of state. The constants m_1 and m_2 characterize various two-parameter cubic equations of state. For the Peng-Robinson equation of state, $m_1 = -1+\sqrt{2}$ and $m_2 = -1-\sqrt{2}$. Equation (1) is integrated with respect to the volume to give the residual Helmholtz energy density (i.e., the difference between the Helmholtz energy of the homogeneous phase and that of an ideal gas). The Helmholtz energy density [J/m^3] is

$$f_{\text{eos,res}} = \frac{R_g T}{v}\ln\left(\frac{v}{v-b}\right) - \frac{a\alpha(T)}{(m_1-m_2)\,bv}\ln\left(\frac{v-m_2 b}{v-m_1 b}\right). \tag{2}$$

The expression is valid if $m_1 \neq m_2$. The Helmholtz energy was further differentiated to give the thermodynamic variables. A complete thermodynamic description of the system was obtained by linking the residuals to the properties of the ideal gas state. A comprehensive consistency check was applied to assure a fully consistent thermodynamic framework.[42]

A. The square gradient model

The square gradient model is frequently used to describe the surface between two phases, also in systems with spherical

symmetries, such as bubbles and droplets.[24,34,43] Since thermodynamic equilibrium in the canonical ensemble is characterized by a minimum in the Helmholtz energy, we find the molar density distributions, c_i, which give a stationary state of the Helmholtz energy functional

$$\overline{F}_{\text{sgm}} = \int_{V_{\text{tot}}} d\mathbf{r} f_{\text{sgm}}(T, \mathbf{c}, \nabla \boldsymbol{c}) = \int_{V_{\text{tot}}} d\mathbf{r} \left(f_{\text{eos}}(T, \boldsymbol{c}) + \frac{1}{2} \sum_{ij=1}^{N_c} \kappa_{ij} \nabla c_i \cdot \nabla c_j \right). \quad (3)$$

Here, subscript sgm refers to the square gradient model. In the following, a bar over the symbol refers to a functional of the whole distribution of the temperature, densities, and the gradients of the densities. $\mathbf{c}$ will be used as short hand notation for the set $\{c_1, \ldots, c_{N_c}\}$ and $\nabla \boldsymbol{c}$ for the set $\{\nabla c_1, \ldots, \nabla c_{N_c}\}$. Bold variables are either vectors or matrices (capital letters). The total number of particles of each component is specified by integral constraints

$$\overline{N_{\text{tot,i}}} = \int_{V_{\text{tot}}} c_i \, d\mathbf{r}. \quad (4)$$

We know from variational calculus that the constrained minimum is a stationary state of the modified functional

$$\overline{\Omega}_{\text{sgm}} = \int_V d\mathbf{r} \left(f_{\text{sgm}}(T, \mathbf{c}, \nabla \boldsymbol{c}) - \sum_i^{N_c} c_i \mu_{\text{sgm},i} \right). \quad (5)$$

Here, $\mu_{\text{sgm},i}$ is the Lagrange multiplier of component i, which is equal to the chemical potential in the square gradient model. Note that, in the canonical ensemble that we are considering, $\mu_{\text{sgm},i}$ is not fixed *a priori*, but it is rather obtained from the stationary density profiles. We used the label "sgm" in Eq. (5) to emphasize this. The Euler-Lagrange equations with integral constraints require that the first variation of $\overline{\Omega}$ is zero, $\delta\overline{\Omega}/\delta c_i = 0$, which gives the following expression for the chemical potentials, if the square gradient parameters, κ_{ij}, are constant:

$$\mu_{\text{sgm},k} = \mu_{\text{eos},k} - \sum_{i=1}^{N_c} \kappa_{ik} \nabla^2 c_i = \mu_{\text{eos},k} - \sum_{i=1}^{N_c} \kappa_{ik} \left(\frac{2}{r} \frac{\partial c_i}{\partial r} + \frac{\partial^2 c_i}{\partial r^2} \right). \quad (6)$$

Note that the square gradient parameters are symmetric. Here, the second line is a simplified expression valid for a system with spherical symmetry around the center, such as in Fig. 1. This can be rewritten in matrix form

$$\mathbf{M}_\kappa \cdot \nabla^2 \mathbf{c} = \boldsymbol{\mu}_{\text{eos}} - \boldsymbol{\mu}_{\text{sgm}}. \quad (7)$$

The matrix $\mathbf{M}_\kappa$ is such that the (i,j) element equals κ_{ij}. Here, $\boldsymbol{\mu}_{\text{sgm}}$ and $\boldsymbol{\mu}_{\text{eos}}$ are the chemical potential vectors. The mixing rule for the square gradient constants is defined according to the most common expression $\kappa_{ij} = \sqrt{\kappa_i \kappa_j}$. This mixing rule is numerically convenient and for many mixtures, it gives accurate predictions of the surface tension. The matrix is then singular with row rank 1, since row i equals row j times $\sqrt{\kappa_i/\kappa_j}$. This allows us to reformulate the multicomponent square gradient model with the structure parameters κ, ε_i, and q

$$\kappa = \kappa_b, \quad (8)$$

$$\varepsilon_i = \sqrt{\frac{\kappa_i}{\kappa}}, \quad (9)$$

$$q = \sum_{i=1}^{N_c} \varepsilon_i c_i. \quad (10)$$

Component b refers to the most abundant one (highest $N_{\text{tot},i}$). We relate the other square gradient parameters to this component through ε_i (note that $\varepsilon_b = 1$). Since the coefficient matrix $\mathbf{M}_\kappa$ has row rank 1, the system of differential equations in Eq. (7) can be reduced to one differential equation and $(N_c - 1)$ algebraic equations

$$\mu_{\text{eos},b} - \mu_{\text{sgm},b} = \kappa \, \nabla^2 q, \quad (11)$$

$$(\boldsymbol{\mu}_{\text{eos}} - \boldsymbol{\mu}_{\text{sgm}}) - \boldsymbol{\varepsilon}(\mu_{\text{eos},b} - \mu_{\text{sgm},b}) = 0. \quad (12)$$

In terms of the order parameters, the state function densities ([J/m^3] and [J/K m^3]) and pressures [Pa] are given as follows:

$$f_{\text{sgm}} = f_{\text{eos}} + \frac{\kappa}{2}(\nabla q)^2, \quad (13)$$

$$u_{\text{sgm}} = u_{\text{eos}} + \frac{\kappa}{2}(\nabla q)^2, \quad (14)$$

$$s_{\text{sgm}} = s_{\text{eos}}, \quad (15)$$

$$h_{\text{sgm}} = h_{\text{eos}} - \kappa q \nabla^2 q, \quad (16)$$

$$g_{\text{sgm}} = g_{\text{eos}} - \kappa q \nabla^2 q, \quad (17)$$

$$P_{\text{sgm}} = P_{\text{sgm},\parallel} = P_{\text{eos}} - \frac{1}{2}\kappa(\nabla q)^2 - \kappa q \nabla^2 q, \quad (18)$$

$$P_{\text{sgm},\perp} = P_{\text{eos}} + \frac{1}{2}\kappa(\nabla q)^2 - \kappa q \nabla^2 q. \quad (19)$$

This treatment of the multicomponent square gradient model is similar as in Ref. 24, which we refer to for further details.

1. Solution method

In addition to the second order partial differential equation, Eq. (11), which can be represented as two first order differential equations, the cumulative mass, $\overline{N_{\text{tot},i}}(r) = 4\pi \int_0^r r^2 c_i dr$, is used as additional variable, satisfying

$$\frac{\partial \overline{N_{\text{tot},i}}}{\partial r} = 4\pi r^2 c_i. \quad (20)$$

The combined system of differential and algebraic equations was solved using the "bvp4c" solver in Matlab, coupled with a multidimensional Newton-Raphson approach to solve the system of algebraic equations at each iteration. The Jacobian matrix of the Newton-Raphson approach was constructed based on the Hessian matrix of the Helmholtz

energy. In addition to the temperature and the total volume, the following $(2+N_c)$ boundary conditions are necessary to fully specify the boundary value problem:

$$\left.\frac{\partial q}{\partial r}\right|_{r=R_{\text{tot}}} = \left.\frac{\partial q}{\partial r}\right|_{r=0} = 0, \tag{21}$$

$$\left.\overline{N_{\text{tot},i}}\right|_{r=R_{\text{tot}}} = N_{\text{tot},i}. \tag{22}$$

The first boundary condition in Eq. (21) means that we have assumed a reflecting wall at $r = R_{\text{tot}}$ with no surface energy. This assumption has been used previously for similar systems,[34] and is expected to have little effect on bubbles/droplets when their radii are much smaller than the container radius. The equimolar dividing surface of component i is defined as[44]

$$0 = \int_0^{R_{\text{tot}}} d\mathbf{r}[c_i(r) - c_i(0)\Theta(R_{n,i} - r) - c_i(R_{\text{tot}})\Theta(r - R_{n,i})]. \tag{23}$$

Here, Θ is the Heaviside step function. We will refer to the equimolar radius, R_n, as the radius where Eq. (23) is satisfied for the total density, $c = \sum_{i=0}^{N_c} c_i$, unless otherwise specified. The densities discussed in this work are scaled with the density of the liquid-phase at coexistence, $c_{\max}$, specified according to Table I. N_{tot} is scaled with the number of moles in a container with homogeneous density $c_{\max}$.

2. Thermodynamic stability analysis of the square gradient model

The square gradient model gives a stationary state of the constrained Helmholtz energy functional, but it is not given whether the state is a minimum, maximum, or a saddle point. This is decided by the second variation, δ_2 which must be positive for a minimum

$$\delta_2\overline{\Omega}_c = \delta_2\overline{F}_c = \frac{1}{2}\int_{V_{\text{tot}}} d\mathbf{r}\sum_{ij}^{N_c}\left(\phi_i\phi_j\left(\frac{\partial\mu_{\text{eos,i}}}{\partial c_{c,j}}\right)_{T,c_{i\neq j}} + \kappa_{ji}\nabla\phi_i\cdot\nabla\phi_j\right) > 0. \tag{24}$$

Subscript c refers to the stationary state. Equality between the second order functional derivatives follows from the linear constraints. Note also that there are no cross terms. At the minimum, this equation should be valid for all functions, ϕ_i, which are sufficiently smooth. Since the constrained number of particles of each component is already given, perturbations of the density profiles cannot introduce additional mass, which means that they should satisfy $\int_{V_{\text{tot}}} d\mathbf{r}\ \phi_{\mathbf{i}} = 0$.

TABLE I. Data used in the simulations. Component 1 is hexane, component 2 is cyclohexane. Surface tension is calculated by the square gradient model for a flat surface, for the mixture at the temperature and composition considered.

Variable	Value
Temperature	330 K
κ_1	4.2×10^{-13} J m^5/kmol^2
κ_2	3.4×10^{-13} J m^5/kmol^2
Overall mole fractions	0.5
Surface tension $_1$	0.144 N/m
Surface tension $_2$	0.205 N/m
Container radius, R_{tot}	38 nm
$c_{\max}$	8.36 kmol/m^3

3. Perturbation functions

We cannot solve Eq. (24) analytically, or test all possible perturbations of the functional numerically to prove that we are at a minimum. By partial integration, Eq. (24) can be reformulated to a vectorial analogue of the eigenvalue problem solved for single-component systems.[35–38] It is challenging to solve the eigenvalue problem numerically for mixtures. Moreover, for apparently positive eigenvalues, we have no guarantee that the smallest eigenvalue has been found, since the problem is not analytical. On the other hand, we only need to find one perturbation which violates Eq. (24) to prove that we are not at a minimum and the state is thermodynamically unstable.

In this work, we will follow another approach. A set of perturbation functions, ϕ will be created. Our hypothesis is that operations which reduce the Helmholtz energy can be approximated by linear combinations of these. A change in the equimolar radii of the bubble/droplet is approximated by a Taylor expansion to first order around the stationary state, which gives the following perturbations:

$$\phi_{R,i} = Q_{R,i}\left(c_{c,i} + d_{R,i}\cdot\nabla c_{c,i}\right) - c_{c,i}. \tag{25}$$

Here, Q_i are normalization constants that satisfy $\int_{V_{\text{tot}}} d\mathbf{r}\ \phi_{\mathbf{i}} = 0$. The distances d_R, determine the sizes of the perturbations. In the case where $d_{R,i} = d_{R,j}$, we call these R-perturbations, since they correspond to a shift in the equimolar surface. In the case where $d_{R,i} \neq d_{R,j}$, but $\sum_i^{N_c} d_{R,i} = 0$, the perturbations affect mainly the composition at the surface. We call these S-perturbations. The bubble/droplet can exchange mass with the surrounding fluid through the following perturbation functions:

$$\phi_{N,i} = Q_{N,i}(c_{c,i} + d_{N,i}(c_{c,i} - c_{c,i}|_{r=R_{\text{tot}}})) - c_{c,i}. \tag{26}$$

The above perturbation functions are called N-perturbations. For typical density profiles of bubbles and droplets, they shift the density of bubbles and droplets compared to the density of the surrounding fluid. The d's in the above equations are constants.

B. The capillary model

Based on previous work on small bubbles and droplets,[29–31,45,46] we define a modified bubble/droplet model, referred to as the capillary model. Let us assume that the bubble/droplet and the exterior both have homogeneous thermodynamic properties separated by an interface at R_n with constant surface tension, σ, with a value which does not depend on R_n. The external phase is connected to a reservoir at temperature, T. The changes in the internal energies of the

gas (g) and liquid phases (l) are

$$dU_{\mathrm{g}} = TdS_g - P_{\mathrm{g}}dV_{\mathrm{g}} + \sum_{i=1}^{Nc} \mu_{\mathrm{g,i}} dN_{\mathrm{g,i}}, \tag{27}$$

$$dU_{\mathrm{l}} = TdS_l - P_{\mathrm{l}}dV_{\mathrm{l}} + \sum_{i=1}^{Nc} \mu_{\mathrm{l,i}} dN_{\mathrm{l,i}} + \sigma dA. \tag{28}$$

Here, A is the area. In this modified capillary model, the surface has been assigned to the liquid phase,[30] contrary to the more sophisticated Gibbs model, where a separate surface phase is identified.[1,47] The total number of moles of each component and the total volume are constant. Moreover, the bubble/droplet is assumed to be perfectly spherical. This gives the following total Helmholtz energy differential:

$$dF_{\mathrm{tot}} = -\left(P_n - P_e - \frac{2\sigma}{R_n}\right) dV_n + \sum_{i=1}^{N_c} (\mu_{\mathrm{n,i}} - \mu_{\mathrm{e,i}}) dN_{\mathrm{n,i}}. \tag{29}$$

Here, we use subscript "n" to denote either a liquid droplet or a bubble at the center of the container, and "e" for the exterior (see Fig. 1). All minima of the Helmholtz energy are characterized by $dF_{tot} = 0$. This leads to equality of the chemical potentials of both phases and the famous Laplace relation

$$P_n - P_e = \frac{2\sigma}{R_n}. \tag{30}$$

The component mass balances for the system give additional algebraic equations to be satisfied

$$\frac{4\pi}{3}\left(c_{n,i}R^3 + c_{e,i}\left(R_{tot}^3 - R_n^3\right)\right) = N_{\mathrm{tot},i}. \tag{31}$$

The Laplace relation and equality of the chemical potentials are necessary conditions for a minimum, but maxima and saddle points satisfy the same conditions, since they are also stationary states of the total Helmholtz energy. We have to investigate the second derivative matrix, **H**, namely, the Hessian of the Helmholtz energy to resolve whether the solution is thermodynamically stable, i.e., a minimum

$$\boldsymbol{H} = \begin{pmatrix} \frac{\partial^2 F_{\mathrm{tot}}}{\partial V_{\mathrm{n}}^2} & \frac{\partial^2 F_{\mathrm{tot}}}{\partial V_n \partial N_{\mathrm{n,1}}} & \cdots & \frac{\partial^2 F_{\mathrm{tot}}}{\partial V_n \partial N_{\mathrm{n,Nc}}} \\ \frac{\partial^2 F_{\mathrm{tot}}}{\partial N_{\mathrm{n,1}} \partial V_{\mathrm{n}}} & \frac{\partial^2 F_{\mathrm{tot}}}{\partial N_{\mathrm{n,1}}^2} & \cdots & \frac{\partial^2 F_{\mathrm{tot}}}{\partial N_{\mathrm{n,1}} \partial N_{\mathrm{n,Nc}}} \\ \vdots & \vdots & \ddots & \vdots \\ \frac{\partial^2 F_{\mathrm{tot}}}{\partial N_{\mathrm{n,Nc}} \partial V_{\mathrm{n}}} & \frac{\partial^2 F_{\mathrm{tot}}}{\partial N_{\mathrm{n,Nc}} \partial N_{\mathrm{n,1}}} & \cdots & \frac{\partial^2 F_{\mathrm{tot}}}{\partial N_{\mathrm{n,Nc}}^2} \end{pmatrix}. \tag{32}$$

Element (1,1) in the matrix is

$$\frac{\partial^2 F_{\mathrm{tot}}}{\partial V_n^2} = -\left(\frac{\partial P_{\mathrm{n}}}{\partial V_{\mathrm{n}}} + \frac{\partial P_{\mathrm{e}}}{\partial V_{\mathrm{e}}} + \frac{\sigma}{2\pi R_n^4}\right). \tag{33}$$

Elements (1,2-N$_c$) and (2-N$_c$,1) are

$$\frac{\partial^2 F_{\mathrm{tot}}}{\partial V_{\mathrm{n}} \partial N_{\mathrm{n,j}}} = \frac{\partial^2 F_{\mathrm{tot}}}{\partial N_{\mathrm{n,j}} \partial V_{\mathrm{n}}} = -\left(\frac{\partial P_n}{\partial N_{n,j}} + \frac{\partial P_e}{\partial N_{\mathrm{e,j}}}\right) = \frac{\partial \mu_{\mathrm{n,j}}}{\partial V_{\mathrm{n}}} + \frac{\partial \mu_{\mathrm{e,j}}}{\partial V_{\mathrm{e}}}, \tag{34}$$

where we have ignored the composition dependence of the surface tension. The rest of the elements are

$$\frac{\partial^2 F_{\mathrm{tot}}}{\partial N_{\mathrm{n,i}} \partial N_{\mathrm{n,j}}} = \frac{\partial \mu_{\mathrm{n,i}}}{\partial N_{n,j}} + \frac{\partial \mu_{\mathrm{e,i}}}{\partial N_{\mathrm{e,j}}}. \tag{35}$$

A minimum is characterized by a positive definite Hessian matrix (positive eigenvalues), a maximum by a negative definite matrix (negative eigenvalues), and a saddle point is characterized by a non-singular indefinite Hessian matrix. A singular Hessian means that higher derivatives have to be investigated. The units of the normalized eigenvectors, v and the corresponding eigenvalues, λ, vary. Since we want to compare to the second variation with units [J], we define the minimum eigenproduct

$$H_{\mathrm{min}} = \frac{1}{2}\min\left(\beta v^T H v \beta\right) = \frac{\beta^2}{2}\lambda_{\mathrm{min}}. \tag{36}$$

Here, β is a dimensionless constant. H_{min} can be interpreted as the smallest second order response to a perturbation in the capillary model. This quantity has the same properties as the smallest eigenvalue and shall be used in Sec. III to determine stability.

Equality of the chemical potential for each component through the system, together with the mass balances and the Laplace equation gives a total of $2N_c$+1 equations, which fully specify the composition of the interior and exterior of the bubble/droplet and the unknown radius. Equation (34) is valid with a constant surface tension. We also tried with a composition dependent surface tension as described in Ref. 31. This had a negligible effect on the results, and the surface tension is hence taken constant in subsequent analysis. In the capillary model, the liquid has been considered as compressible, and its compressibility is determined from the Peng-Robinson equation of state.

III. RESULTS AND DISCUSSION

Although the formulation in Sec. II has been derived for multicomponent systems, for simplicity, results will be particularized for the binary system, hexane-cyclohexane, because this has been popular in the literature.[34,48] We have investigated the single-component systems and the two-component system with several overall compositions. Since all the systems have the same qualitative behavior, we present results only for the 50% hexane-cyclohexane mixture in the figures.

Parameters of the models can be found in Table I. The square gradient parameters, κ_1 and κ_2, were chosen such that they reproduce exactly the surface tension reported for the single-component systems hexane and cyclohexane at 300 K.[49] The surface tension used in the capillary model, reported in Table I, is that predicted by the square gradient model for a planar surface.

Figs. 2 and 3 show density profiles of three bubble-like and droplet-like cases. We refer to cases where the density in the center is lower than at R_{tot} as bubble-like and the opposite situation as droplet-like. First, let us discuss the possible stationary states of the square gradient model, and whether they can be reproduced by the capillary model. For the stable bubbles and droplets (solid lines in Figs. 2 and 3), the density

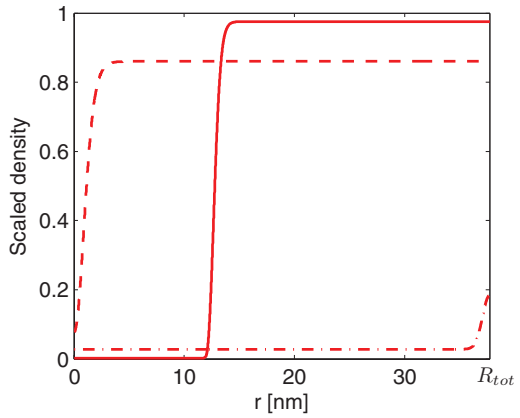

FIG. 2. Bubble density profiles from the square gradient model. Stable bubble, $N_{\text{tot,s}} = 0.82$ (solid line). Unstable bubble, $N_{\text{tot,s}} = 0.86$ (dashed line). Unstable bubble, $N_{\text{tot,s}} = 0.04$ (dashed-dotted line).

changes from approximately the equilibrium liquid density in one phase, to approximately the equilibrium vapor density in the other. For smaller bubbles and droplets which are thermodynamically stable, these densities change only moderately, as shown in Fig. 1 in previous work.[34]

From the dashed lines in Figs. 2 and 3, it is clear that we can obtain density profiles where the size of the bubble/droplet is comparable to the thickness of the surface, even if these solutions are thermodynamically unstable, as we will discuss later. The profiles represented by the dashed-dotted lines are not easily characterized as bubbles or droplets, but are nonetheless stationary states of the square gradient model. Even if it is not clear from the figures, a zooming in near $r = 0$ and $r = R_{\text{tot}}$ shows that $\partial c/\partial r = 0$.

At 330 K, the 50% hexane-cyclohexane system gives stationary states which vary with the total number of particles as shown in Fig. 4(a) for the capillary model and Fig. 4(b) for the square gradient model. Both single-component systems and two-component systems with all compositions investigated display qualitatively the same behavior as shown in these figures. It has, to the best of our knowledge, not been shown before that the solutions of the square gradient model representing bubbles and droplets can be connected in a closed loop as in Fig. 4(b). This shows the importance of considering bubbles and droplets as connected phenomena, instead of treating them separately according to the most common procedure. The figures show that four stationary states are possible for given values of the scaled total mass in the container.

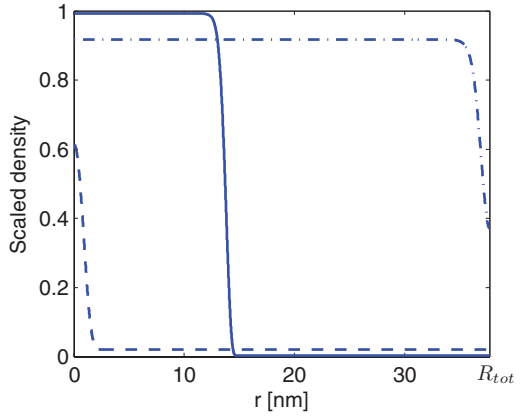

FIG. 3. Droplet density profiles from the square gradient model. Stable droplet, $N_{\text{tot,s}} = 0.47$ (solid line). Unstable droplet, $N_{\text{tot,s}} = 0.02$ (dashed line). Unstable droplet, $N_{\text{tot,s}} = 0.87$ (dashed-dotted line).

The bubble-like solutions transform into droplet-like solutions at the bullet points where the dashed lines meet the solid lines. This corresponds exactly to the spinodal points (see vertical dashed-dotted lines in Fig. 4(b)). At the spinodal, the radius of the bubble/droplet diverges, since the solution of the square gradient model is a homogeneous density profile at that point. Equation (23) will, however, give a finite radius. The divergence of the square gradient model and density functional theory at the spinodals is well known and has been discussed in previous work (see Ref. 50 and references therein). The symmetry of the stationary solutions is striking. This symmetry is also reflected in the thermodynamic stability of bubbles and droplets. Note that the bullet points in the top part of Fig. 4 may at first sight look unsymmetrical. A closer investigation reveals that they are both located before the curves turn over.

The capillary model reproduces very well the stable bubble and droplet solution in the whole range of masses. For the unstable branches, corresponding to the critical clusters, the capillary model reproduces well the bubble and droplet radii predicted by the square gradient method until scaled masses of $N_{\text{tot},s} \sim 0.81$ and $N_{\text{tot},s} \sim 0.03$ according to Fig. 4. Other quantities like pressures, densities, and compositions are also well reproduced,[51] given that the same surface tension is used in the capillary model, as predicted by the square gradient model for a planar surface. In fact, if the lines in Figs. 4(a) and 4(b) are placed on top of each other, they are so similar for large parts of the diagram that they can hardly be distinguished from each other before they separate near the spinodals.

After they separate, the radii of the solutions of the square gradient model follow nearly vertical lines in Fig. 4(b) which reconnect to form a closed loop. The solutions of the capillary model continue nearly horizontally and diverge. The reason for this divergent behavior is that the surface tension in the capillary model is fixed. In the square gradient model, the surface tension drops quickly after the minimum bubble/droplet radii have been reached, and drops to zero at the spinodal. The capillary model predicts a non-diverging radius at and also beyond the spinodal points, but both phases are here mechanically unstable (thin lines in Fig. 4(a)). These solutions have no physical meaning.

It is possible that there are more stationary states of the square gradient model than those presented in Fig. 4(b). For instance, the trivial homogeneous solution of the square gradient model with homogeneous densities for all components is not represented in the figures. The trivial solution is thermodynamically locally stable on both sides outside of the region enclosed by the spinodal points. With an overall composition which lies within this region, however, a bubble or droplet will form. Remarkably, both the capillary and the square gradient model predict the existence of a minimal radius of stable bubbles and droplets. Thus, as in the single-component case,[34,51]

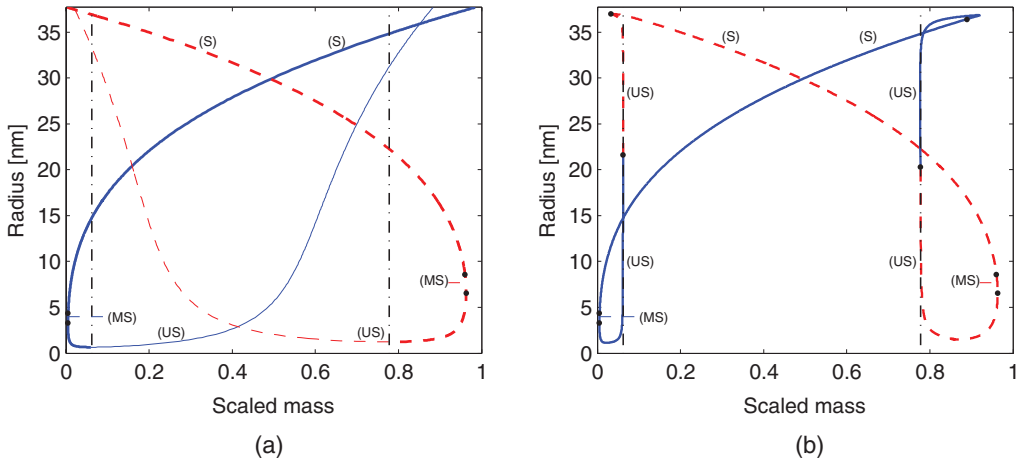

FIG. 4. (a) Capillary model and (b) square gradient model: Radii of the solutions of the two models as function of the scaled total number of moles. Bubble-like solutions (red dashed lines) and droplet-like solutions (blue solid lines). The spinodal compositions (dashed-dotted lines). Thin lines in the capillary model mean that both bubble/droplet and surrounding fluid are mechanically unstable. The bullet points denote a change in thermodynamic stability or nature of solution, with US: Unstable, S: Stable, MS: Metastable.

it is not possible to stabilize very small bubbles and droplets, not even in closed systems.

A. Thermodynamic stability

To investigate the thermodynamic stability involves analyzing the eigenvalues of the Hessian matrix in the capillary model, and the second variation in the square gradient model as explained in Sec. II.

First, let us examine the eigenvalues and eigenvectors of the Hessian matrix in the capillary model. The eigenvectors can be interpreted for the stationary states representing bubbles, but are more convoluted for droplets. One eigenvalue corresponds to a change in the bubble radius with little exchange of mass. The next N_c eigenvalues correspond mainly to exchange of mass from the bubble/droplet to the surrounding fluid. Our hypothesis is that the operations represented by these eigenvectors, and also other relevant operations can be reproduced in the square gradient model by linear combinations of the N,R,S-perturbations described in Sec. II. Since the surface tension is fixed in the capillary model, we cannot change the properties of the surface. This means that the S-perturbation which changes the composition at the surface has no equivalent in the capillary model.

In the bottom parts of Figs. 4(a) and 4(b), the bubbles and droplets go from stable/metastable to unstable. Figs. 5(a) and 5(d) compare the minimum eigenproduct of the Hessian-matrix in the capillary model with the second variation of the square gradient model in the transition from stable to unstable.

Figs. 5(b) and 5(d) present results with linear combinations of the S,R and N-perturbations giving the smallest possible value of the second variation. The prefactor in the minimum eigenproduct was specified according to $\beta \propto \Delta V_n \approx (A_n d_R)$, such that the length of the eigenvectors of the minimum eigenproduct corresponds with the perturbation invoked in the square gradient model. This allows us to compare the response of perturbations in the two models also quantitatively.

By comparing Figs. 5(a)–5(d), the smallest second variation is a remarkably good approximation of the minimum eigenproduct. In particular, they shift from stable to unstable in exactly the same point. In the stability analysis of the square gradient model, the main role of the R-perturbation is to shift the surface. The role of the N-perturbations is to change the densities inside and outside the bubble/droplet without moving the surface. The S-perturbation mainly changes the properties of the surface. We found that the perturbation which gave the smallest second variation, was a superposition of the R and the N-perturbations such that the density in the bubble/droplet remained the same. Many superpositions of perturbations gave negative second variations and destabilized the stationary solution in the unstable region, however, the combination above destabilized bubbles and droplets at the highest and lowest values of the total mass in the system, respectively (see Fig. 4).

The S-perturbations, which change the properties of the surface, were found to increase the second variation in all cases investigated. This means that the properties of the surface found by the square gradient model attain a minimum surface energy and only a displacement of the surface leads to a destabilization.

The largest eigenvalue of the capillary model always stays positive, meaning that the unstable solutions are saddle points. This is also the case for the second variation, where we could always find linear combinations of perturbations which gave both positive and negative values in the unstable region.

The difference in Helmholtz energy between a system with a bubble or a droplet and a supersaturated gas or undersaturated liquid, ΔW, is known as the reversible work of formation. We refer to thermodynamically locally stable states where ΔW is positive as metastable. Metastable systems with small bubbles and droplets have higher energies than a homogeneous fluid, but are stable to perturbations, i.e., local minima. Before the solutions change from stable to unstable in the bottom parts of Figs. 4(a) and 4(b), the bubbles and droplets are metastable with respect to the homogeneous

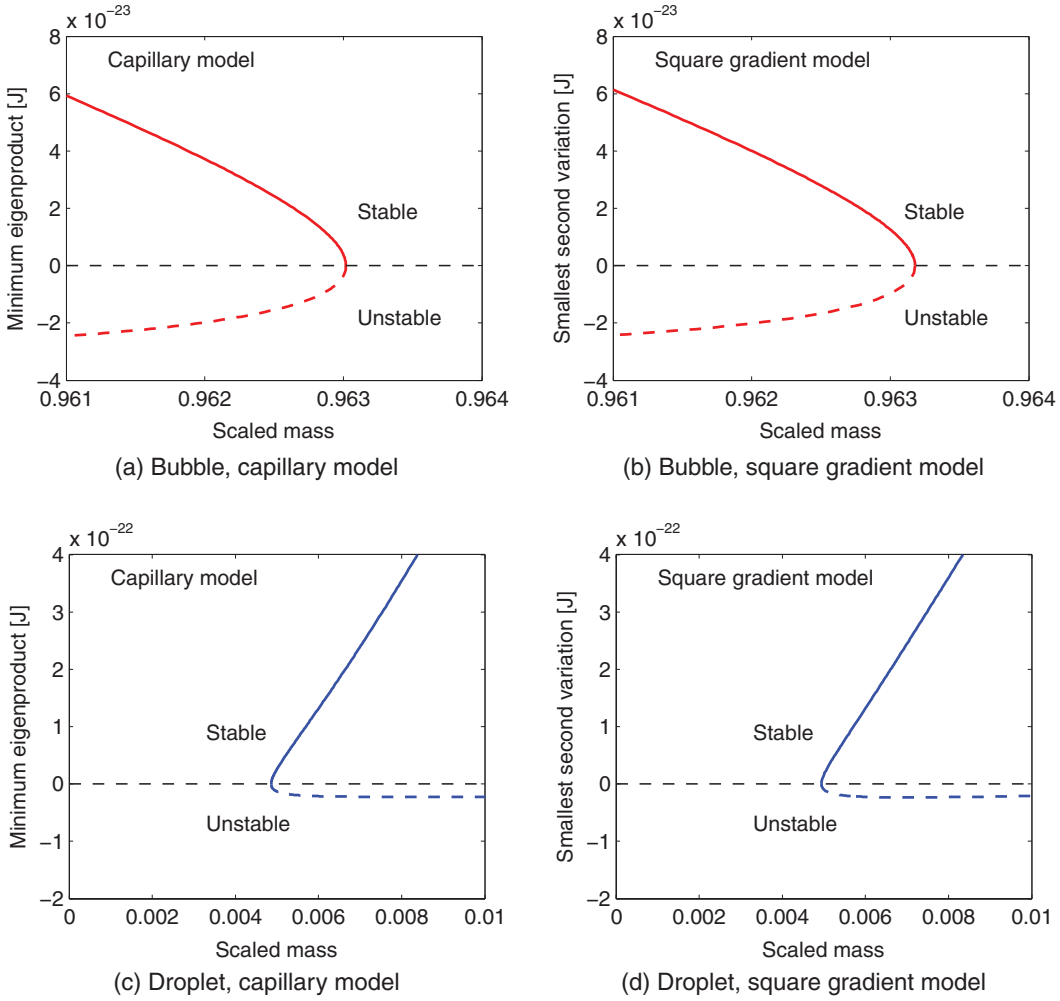

FIG. 5. Comparison of the minimum eigenproduct in the capillary model (a) and (c), with the smallest second variation obtained in the square gradient model (b) and (d) for model for 50% hexane-cyclohexane.

state.[29,30] This can be seen from Figs. 6(a) and 6(b). They show results from both models, since ΔW is close to identical for the square gradient model and the capillary model. Notice the similar behavior of bubbles and droplets in Figs. 6(a) and 6(b). Other authors have also found metastable droplets,[30] while metastable regions for bubbles are rarely mentioned in the literature.

In the region between the spinodal points, both bubbles and droplets are stable. Medium sized droplets, however, have higher Helmholtz energies than systems with large bubbles

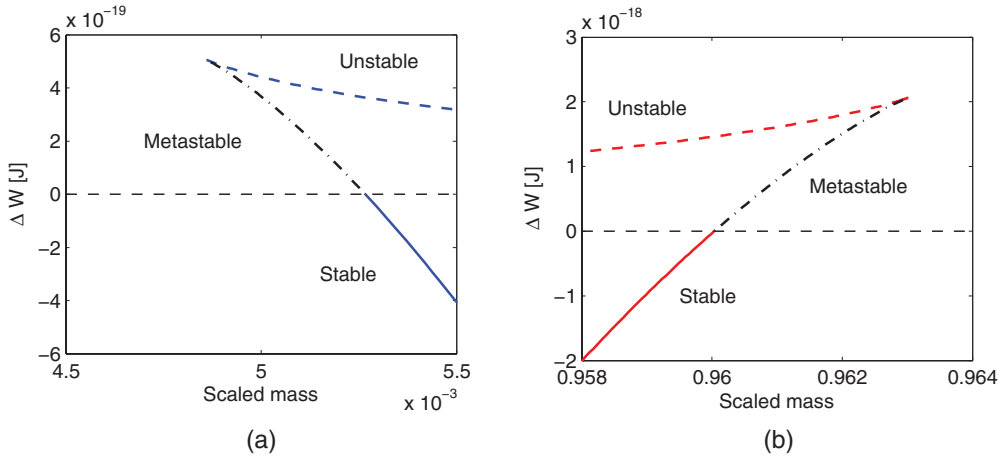

FIG. 6. (a) The droplet and (b) the bubble: The reversible work of formation near the transition between the stable/unstable solutions of hexane-cyclohexane. The solutions are stable (solid lines), metastable (dashed-dotted lines), and unstable (dashed lines).

below a scaled mass, $N_{\text{tot},s} \sim 0.49$, and systems with medium sized bubbles have higher Helmholtz energies than systems with large droplets at scaled masses above $N_{\text{tot},s} \sim 0.49$. This is the point where the dashed and solid lines cross in Fig. 4. It is energetically favorable for the system to form bubbles when the homogenous fluid is vapor-like, and favorable to form droplets when the fluid is liquid-like.

IV. CONCLUSION

In this paper, we have investigated the formation and stability of nanoscale multicomponent bubbles and droplets in a closed container. We have seen that there exists a minimum threshold radius for their formation in the canonical ensemble. We used the square gradient model for curved systems to analyze the system from a mesoscopic point of view, and compared the results to those obtained from the capillary model, which addresses the problem from a macroscopic point of view. For the hexane-cyclohexane mixture, the capillary model was able to reproduce the results from the square gradient model in the stable regions well, if the value for the surface tension obtained from the square gradient model for a planar surface was used. The solutions of the square gradient model formed closed loops, which emphasizes the symmetric and connected nature of bubbles and droplets.

The eigenvalue of the Hessian matrix in the capillary model, and the second variation in the square gradient model was used to analyze the thermodynamic stability. For all investigated systems, the same stability limits were found in the capillary model and the square gradient model away from the spinodals, given that the size of the bubble/droplet was not close to the size of the container. Metastable regions were located in both models before the minimum threshold radii. The impossibility of forming very small drops and bubbles in multicomponent systems has important implications on nucleation that will be explored in a future work.

ACKNOWLEDGMENTS

The authors thank the Faculty of Natural Sciences and Technology at the Norwegian University of Science and Technology for the Ph.D.-grant of Øivind Wilhelmsen. The work was partially supported by the Spanish MINECO through Grant No. FIS2011-22603 co-financed by European Union's (EU) FEDER funds.

[1] S. Kjelstrup and D. Bedeaux, *Non-equilibrium Thermodynamics of Heterogeneous Systems* (World-Scientific, 2008).
[2] Ø. Wilhelmsen, G. Skaugen, M. Hammer, P. E. Wahl, and J. Morud, Ind. Eng. Chem. Res. **52**(5), 2130 (2013).
[3] H. Vehkamäki, *Classical Nucleation Theory in Multicomponent Systems* (Springer, 2006).
[4] U. Gasser, E. R. Weeks, A. Schofield, P. N. Pusey, and D. A. Weitz, Science **292**(5515), 258 (2001).
[5] S. T. Tau and P. G. Vekilov, Nature (London) **406**, 494 (2000).
[6] A. Lervik, F. Bresme, and S. Kjelstrup, Soft Matter **5**, 2407 (2009).
[7] P. G. Debenedetti, *Metastable Liquids*, edited by Princeton (Princeton University Press, 1996).
[8] V. I. Kalikmanov, *Nucleation Theory*, edited by Berlin (Springer Verlag, 2013).
[9] R. Strey, P. E. Wagner, and T. Schmeling, J. Chem. Phys. **84**(4), 2325 (1986).
[10] C. Hung, M. J. Krasnopoler, and J. L. Katz, J. Chem. Phys. **90**(3), 1856 (1989).
[11] B. E. Wyslouzil, J. H. Seinfeld, R. C. Flagan, and K. Okuyama, J. Chem. Phys. **94**, 6827 (1991).
[12] K. Iland, J. Wölk, R. Strey, and D. Kashchiev, J. Chem. Phys. **127**(15), 154506 (2007).
[13] J. K. Lee, J. A. Barker, and F. F. Abraham, J. Chem. Phys. **58**(8), 3166 (1973).
[14] M. Rao, B. J. Berne, and M. H. Kalos, J. Chem. Phys. **68**(4), 1325 (1978).
[15] B. Chen, J. I. Siepmann, J. O. Kwang, and M. L. Klein, J. Chem. Phys. **115**(23), 10903 (2001).
[16] S. Auer and D. Frenkel, Nature (London) **409**, 1020 (2001).
[17] L. G. MacDowell, V. K. Shen, and J. R. Errington, J. Chem. Phys. **125**(3), 034705 (2006).
[18] J. Wedekind, J. Wölk, D. Reguera, and R. Strey, J. Chem. Phys. **127**(15), 154515 (2007).
[19] B. N. Hale and M. Thomason, Phys. Rev. Lett. **105**, 046101 (2010).
[20] J. Diemand, R. Angílil, K. Tanaka, and H. Tanaka, J. Chem. Phys. **139**(7), 074309 (2013).
[21] J. S. Rowlinson, J. Stat. Phys. **20**(2), 197 (1979).
[22] J. W. Cahn and J. E. Hillard, J. Chem. Phys. **28**(2), 258 (1958).
[23] D. Bedeaux, E. Johannessen, and A. Røsjorde, Physica A **330**(3), 329 (2003).
[24] K. Glavatskiy, "Multicomponent interfacial transport described by the square gradient model during evaporation and condensation," Ph.D. thesis, Norwegian University of Science and Technology, 2009.
[25] L. Granasy, J. Non-Cryst. Solids **162**(3), 301 (1993).
[26] E. Johannessen and D. Bedeaux, Physica A **336**(4), 252 (2004).
[27] E. Johannessen and D. Bedeaux, Physica A **370**(2), 258 (2006).
[28] K. Glavatskiy and D. Bedeaux, J. Chem. Phys. **133**(23), 234501 (2010).
[29] A. J. M. Yang, J. Chem. Phys. **82**, 2082 (1985).
[30] D. Reguera, R. K. Bowles, Y. Djikaev, and H. Reiss, J. Chem. Phys. **118**, 340 (2003).
[31] D. Reguera and H. Reiss, J. Chem. Phys. **119**, 1533 (2003).
[32] D. Reguera and H. Reiss, Phys. Rev. Lett. **93**(16), 165701 (2004).
[33] D. J. Lee, M. M. Telo de Gama, and K. E. Gubbins, J. Chem. Phys. **85**(1), 490 (1986).
[34] K. Glavatskiy, D. Reguera, and D. Bedeaux, J. Chem. Phys. **138**(20), 204708 (2013).
[35] M. S. Wertheim, J. Chem. Phys. **65**(6), 2377 (1976).
[36] D. J. Bukman, A. B. Kolomeisky, and B. Widom, Colloids Surf. A **128**(1–3), 119 (1997).
[37] C. Varea and A. Robledo, Physica A **255**(3–4), 269 (1998).
[38] M. Iwamatsu and Y. Okabe, J. Chem. Phys. **133**(4), 044706 (2010).
[39] D. Y. Peng and B. R. Robindon, Ind. Eng. Chem. Fundam. **15**(1), 59 (1976).
[40] H. Li, P. J. Jakobsen, Ø. Wilhelmsen, and J. Yan, Appl. Energy **88**(11), 3567 (2011).
[41] Ø. Wilhelmsen, G. Skaugen, O. Jørstad, and H. Li, Energy Proc. **23**, 236 (2012).
[42] M. L. Michelsen and J. M. Mollerup, *Thermodynamic Models: Fundamentals and Computational Aspects* (Tie-Line Publications, 2007).
[43] J. Hruby, D. G. Labetski, and M. E. van Dongen, J. Chem. Phys. **127**(16), 164720 (2007).
[44] P. R. ten Wolde, "Numerical study of pathways for homogeneous nucleation," Ph.D. thesis, University of Amsterdam, 1998.
[45] V. Talanquer and D. W. Oxtoby, J. Chem. Phys. **102**(5), 2156 (1995).
[46] A. Laaksonen, R. McGraw, and H. Vehkamäki, J. Chem. Phys. **111**(5), 2019 (1999).
[47] G. Wilemski, J. Chem. Phys. **80**(3), 1370 (1984).
[48] I. Inzoli, S. Kjelstrup, D. Bedeaux, and J. M. Simon, Chem. Eng. Sci. **66**(20), 4533 (2011).
[49] J. J. Jasper, J. Phys. Chem. Ref. Data. **1**(4), 841 (1972).
[50] G. Wilemski and J. S. Li, J. Chem. Phys. **121**(16), 7821 (2004).
[51] Ø. Wilhelmsen, D. Bedeaux, S. Kjelstrup, and D. Reguera, in Proceedings of JETC-13, 2013.